applied sciences

MDPI

Article

Analysis of the Pressure Increase in the Hydraulic Cylinder of the Longwall Powered Roof Support during Use

Dawid Szurgacz [1,2]

[1] Center of Hydraulics DOH Ltd., ul. Konstytucji 147, 41-906 Bytom, Poland; dawidszurgacz@vp.pl
[2] Polska Grupa Górnicza S.A., ul. Powstańców 30, 40-039 Katowice, Poland

Abstract: This paper presents the results of lab-simulated tests on longwall powered supports under dynamic loading conditions. The tests were carried out on a test site, where the tested prop was subjected to a dynamic load using a controlled mass falling under gravity onto the support. The loading on the support was therefore determined based on the weight used and the distance of freefall before impact. The operating characteristics of the valve were determined, specifying temporary changes in the pressure and the prop's dynamic yield rate and total deformation. The research aimed to determine the operational parameters of the valve to be used in new and improved components for powered roof supports. One of the most essential elements of the powered roof support hydraulic system is the safety valve. The results confirm the validity of the concept and the possibility of applying the tested valve to the developed control system of the prop of the powered roof support. The forged safety valve has been designed to significantly improve the safety and efficiency of the powered roof support, especially in conditions of safety hazards.

Keywords: bench research; powered roof support; safety valve; work safety

Citation: Szurgacz, D. Analysis of the Pressure Increase in the Hydraulic Cylinder of the Longwall Powered Roof Support during Use. *Appl. Sci.* **2022**, *12*, 8806. https://doi.org/10.3390/app12178806

Academic Editor: Radosław Zimroz

Received: 13 August 2022
Accepted: 28 August 2022
Published: 1 September 2022

1. Introduction

Currently, research is being carried out worldwide regarding the development of modern technologies related to coal mining in open-cast and underground mines [1–3]. Based on the literature, four main research areas related to coal mining have been defined [4–6]. The first focuses on machines related to haulage [7–9], and the second is related to coal mining machines [10–12]. However, in the third area, research problems related to the development of powered roof supports have been considered [13–15]. The fourth area includes machines and devices complementary to ongoing exploitation [16–18].

Coal is the primary energy resource in many countries [19–21]. The effective and safe extraction of hard coal occurs mainly through underground mines' longwall systems [22–24]. The latest systems [25–27] operate in a fully automated way and are controlled by an electro-hydraulic system [28–30]. The powered roof support is an essential piece of the equipment suite needed for longwall mining [31]. It is responsible for the safety of the workforce and equipment [32–34], and it is also important to move the armored face conveyor and shearer forward as mining progresses [35–46]. A particular requirement for the powered roof support [47–49] is to ensure the safety of the excavation [50–52] in case of a violent coal burst or bump [53,54] (mining-induced seismic event or earthquake).

Under dynamic loading from localized seismicity, the support is able to rapidly yield whilst maintaining a reactive load in the immediate roof because of the safety valve in each hydraulic cylinder [55,56]. These are used to control the stiffness and yield in the cylinder to prevent the overloading and failure of the support [57,58]. The fundamental parameter characterizing the safety valve is its mass flow rate depending on the supply pressure [59,60]. Determining such dependence through research is significantly challenging due to the need for a power source with an MW value through calculations [61]. However, this is burdened with a significant error due to the enormous and rapidly induced dynamics of the flows (Reynolds number $> 1 \times 10^6$) of the liquid in the valve [62].

From the converted teaching experience [63] considered in the literature [64] on safety engineering [65], we have adopted an interactive view [66] to solve technical problems [67]. This allows the adoption of already-described methods for assessing the suitability of structures [68].

The main task of the powered roof support is to maintain excavation stability. A typical longwall shield is shown in Figure 1. This is done by transferring the load resulting from the pressure of the rock layers on the immediate roof through the hydraulic legs into the floor. Thus, the powered roof support should be able to accommodate quasi-static and dynamic loads. The essential elements of each powered roof support are the roof, the stringer, the shield system and the props. Hydraulic props determine the stability and maintenance of the powered roof support. Protecting the hydraulic prop against adverse overload is achieved through the safety valve.

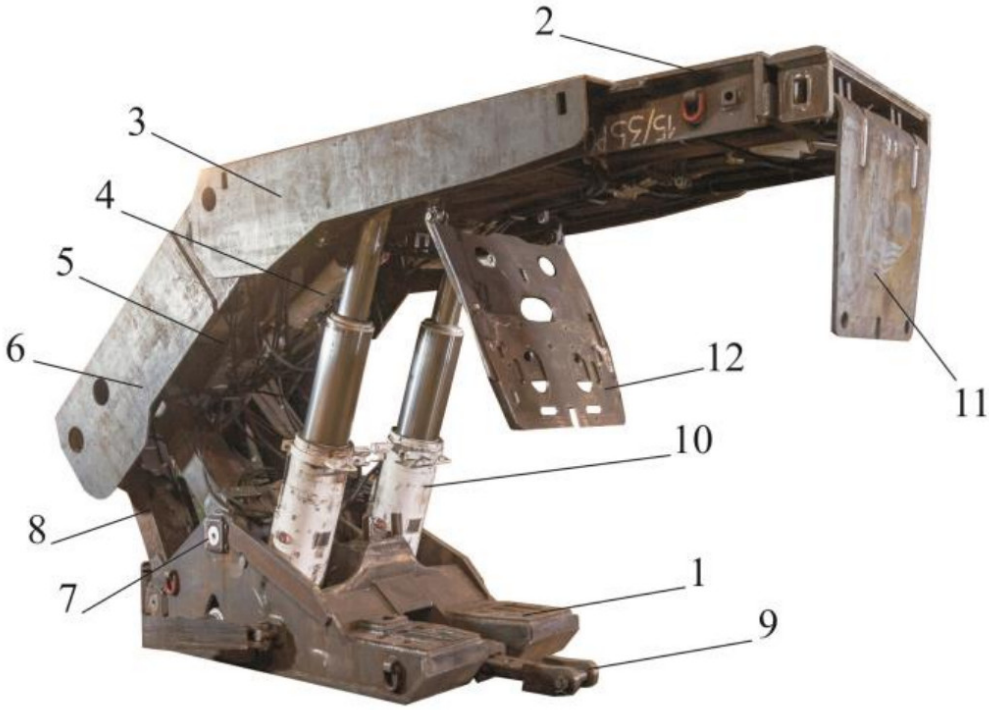

Figure 1. Longwall powered roof support, where: 1—floor base, 2—canopy, 3—lateral shield of canopy, 4—ceiling support actuator, 5—shield support, 6—lateral shield of shield support, 7—top lemniscate tie rods, 8—lower lemniscate tie rods, 9—beam of sliding system, 10—leg, 11—wall face cover, 12—crew walkway cover.

This paper presents research regarding possible damage to the support as a result of the dynamic loading of the rock mass. Damage to the hydraulic cylinder of the powered roof support prop (Figure 2) can occur due to this sudden loading in the longwall. The energy of the rock mass 6×10^6 J had a significant impact on the time of opening the safety valve. In this case, the resulting crack of the prop and the recorded pressure (Figure 3) in the sub-piston space showed the following results:

- Insufficient flow rate in the hydraulic system of the prop;
- Its inclination is too high when working in the extraction longwall;
- An overload of the prop due to component defects;
- Incorrect configuration/settings of the control system;
- Too little hydraulic fluid in the piston of the prop;
- Malfunction or failure of the safety valve.

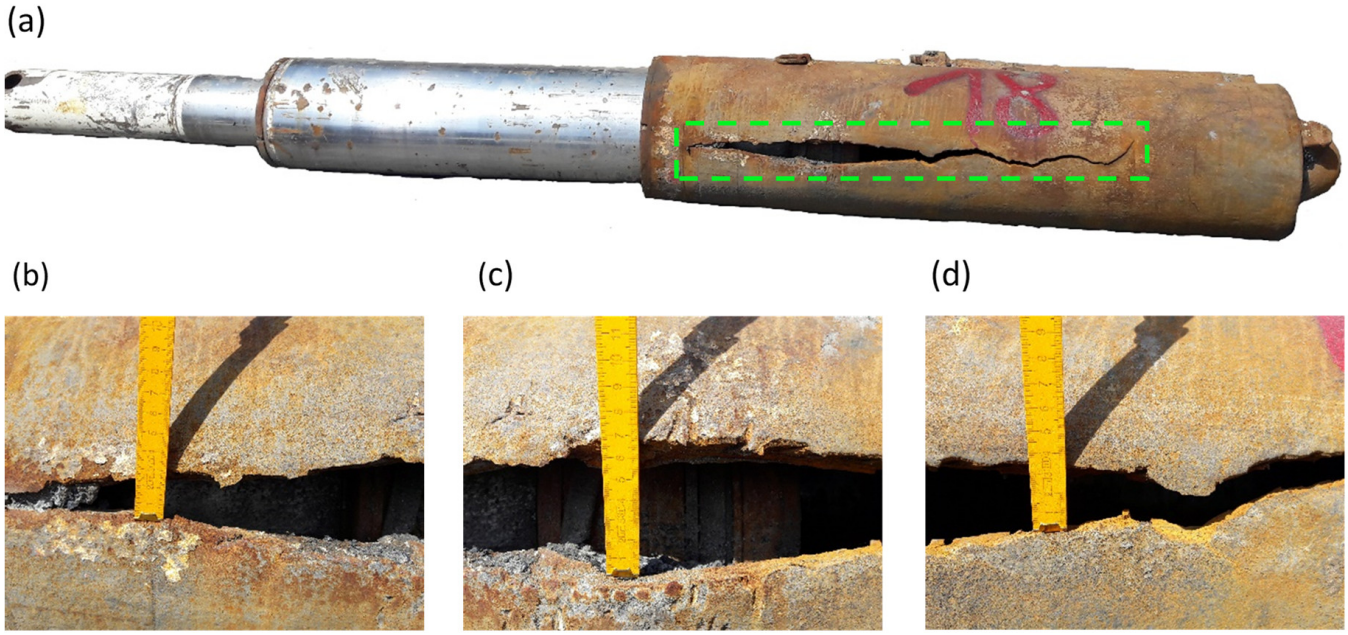

Figure 2. Damaged cylinder of the first stage of a double-telescopic hydraulic leg, where: (**a**) crack area (**b**) area of minimal cracking in the initial phase, (**c**) maximum crack area, (**d**) final rupture area.

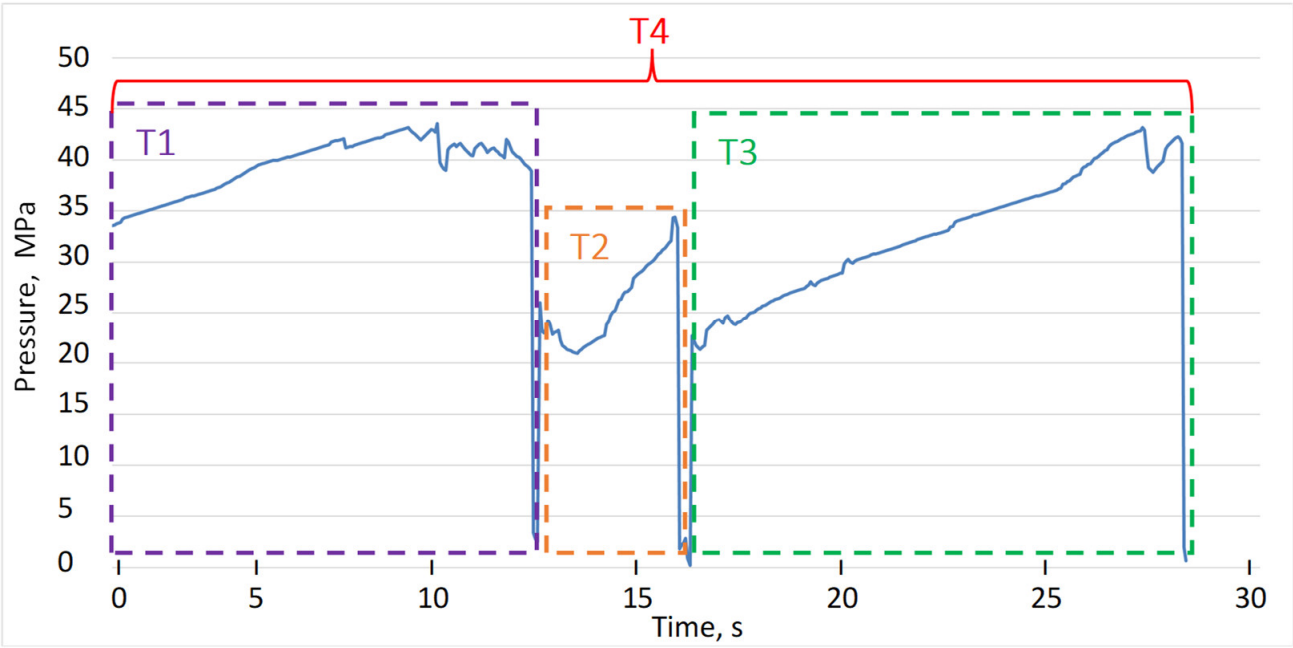

Figure 3. Recorded pressure during the rock mass shock that caused the rack to fail.

The dynamic phenomenon causing damage to the prop is the sudden shock loading and movement of rock mass with the energy of 6×10^6 J. Figure 3 shows the operation of the damaged prop. From the graph, it can be concluded that the time of the load in T1 was 13 s. In T2, this time was 5 s. The course of the dynamic impact of the rock mass in T3 caused its maximum load after 13 s, which was manifested by an increase in the pressure of the liquid in the under-pistol space to 45 MPa. The time in T4 covers the entire period of dynamic loading, and is the duration of the phenomenon.

Based on the analysis of the above drawings (Figures 2 and 3), an attempt was made to analyses the pressure increase in the safety valve during shock loading. The tests used a hydraulic cylinder (from the powered roof support) loaded using a freefalling mass. Such

loading systems are commonly used for coal longwall shield testing and are available, for example, in Poland and the Czech Republic. The research concept and its implementation required the preparation of an appropriate actuator, measuring and recording equipment, and a sound methodology. This paper presents the results using this research methodology. A pressure increase in the safety valve using this method was determined.

2. Materials and Methods

The methodology for determining the mass flows of the hydraulic valve used a ram bench (dynamic load with a mass impact). The hydraulic valve mass flow, according to the methodology used, is described by binding the pressure at the valve inlet to the liquid mass flow through the valve P = f(Q). The characteristics are determined in the position schematically presented in Figure 5. The impact mass (1) dynamically loads the standard prop (7) expanded in the station. The standard prop is connected to the valve (9) and the converter of the pressure and displacement of the actuator rod (5). The dynamic loading of the actuator by the impact of the mass causes an increase in pressure in the under-piston space. Then, the valve's flow opens, and liquid flows out of the valve connected to the actuator. We recorded the pressure under piston *P(t)* and a slip as a function of time *l(t)*. We obtained high values of the *P(t)* and *l(t)* functions based on the recorded actuator slips. Knowing the surface of the cylinder of the actuator, we can determine the value of liquid flow through the valve *Q(t)* depending on the time from the relation:

$$Q(t) = l(t) \cdot S_s, \mathrm{m^3 s^{-1}}, \quad (1)$$

where:

l(t)—clamping speed of the cylinder (derivative of path with respect to time), $\mathrm{ms^{-1}}$;
S_s—cylinder surface of the calibrated cylinder, $\mathrm{m^2}$.

The designated functions describing the inlet pressure of the valve $P(t)$ and the mass flow $Q(t)$ are the basis for determining the desired function describing the flow in the hydraulic valve $P = f(Q)$. Depending on the technical parameters of the valve, we selected the actuator (cylinder surface) and the value of the impact energy in such a way as to obtain the appropriate pressure at the valve inlet and mass flow. Tests to determine the flow characteristics of the valve were performed in chapter 3 for the adopted valve data. The piston-type valve (Figure 5) was a circular gasket spring with a diameter of Ø14 mm. Its opening pressure was 21 MPa.

The authors used a custom designed system to carry out the measurements and record the test results [69]. The measurement system was built with a control and intermediary module that allows for pressure and movement measurements with time. It was developed using a cRIO9030 card from National Instruments. The layout module was equipped with two different operator interfaces. Communication was via an Ethernet link. The measurement system was connected to a PC, which was equipped with appropriate software made by LabVIEW environment. The research was conducted at two research centers in TLO Opava (Czech Republic) and the (Figure 4) Central Mining Institute (Poland).

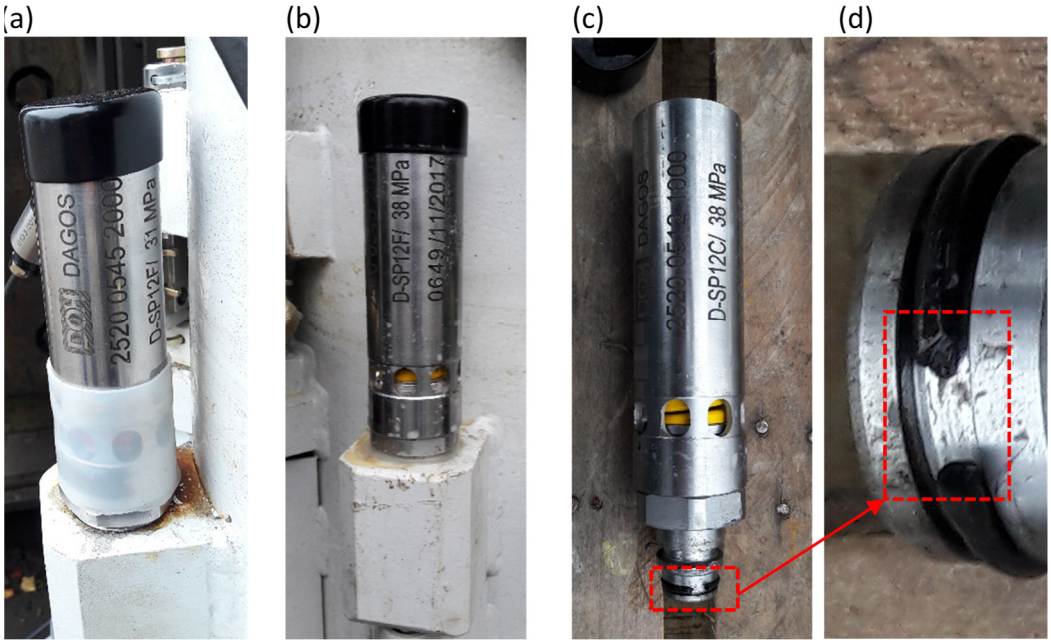

Figure 4. View of tested valve, where: (**a**) valve before test, (**b**) valve after test, (**c**,**d**) damaged gasket after test.

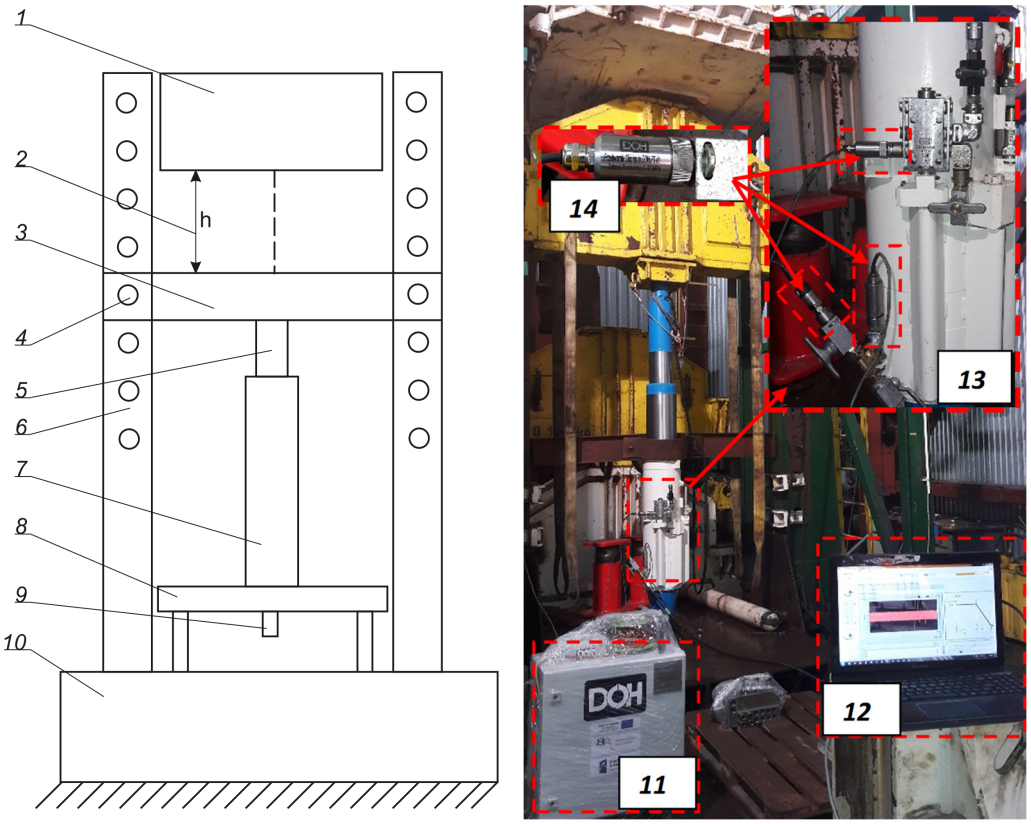

Figure 5. Scheme of the testing station, where: 1—impact mass 20,000 kg, 2—slope height, 3—traverse 3300 kg, 4—crosshead locking pin in the stand frame, 5—hydraulic piston rod, 6—impact mass slides, 7—hydraulic stand cylinder with pressure sensor, 8—basis of the position, 9—the valve to be tested fixed in the bottom of the leg cylinder, 10—foundation of the position, 11—innovative measuring and recording system, 12—computer PC, 13—hydraulic system under test, 14—pressure sensor.

3. Results

The safety valve test used to determine its flow characteristics consisted of converting the kinetic energy loading the prop for the operation of its release (and yield) at the specified speed of this dynamic loading. The energy transferred during the bench test to the prop also causes movement when the load no longer impacts this prop. The speed of movement of the prop piston forces the appropriate flow rate of liquid from the prop sub-piston space. The safety valve to be tested and the prop shall ensure an adequate liquid flow rate such that the cylinder does not fail due to over-loading. In the following test results (Figure 6), it is possible to observe that with a lower the flow rate of liquid through the valve than the flow rate of the piston forced by the movement of the prop, a greater increase in the pressure of the liquid in the space under the piston rod of the hydraulic leg will be obtained (Figure 7).

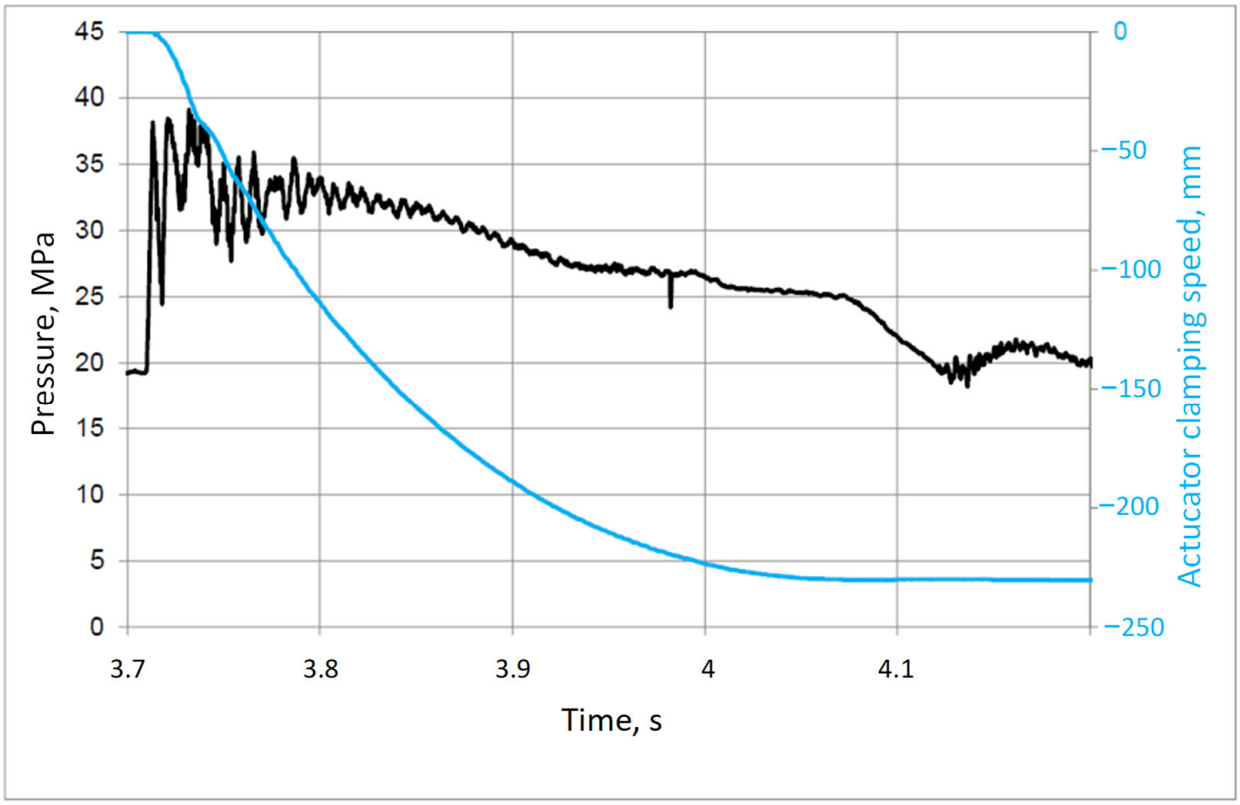

Figure 6. Recorded pressure waveform on valve input P(t) and retraction of the hydraulic cylinder piston rod l(t).

Based on the recorded progress shown in Figures 6 and 7, the actuator clamping speed was determined as the slip difference (derivative). After multiplication by its surface, the flow in relation to time was obtained per the relationship (1). The averaged values made it possible to determine the dependence of pressure on the values of computational time flows according to the relations (1), as shown in Figure 8.

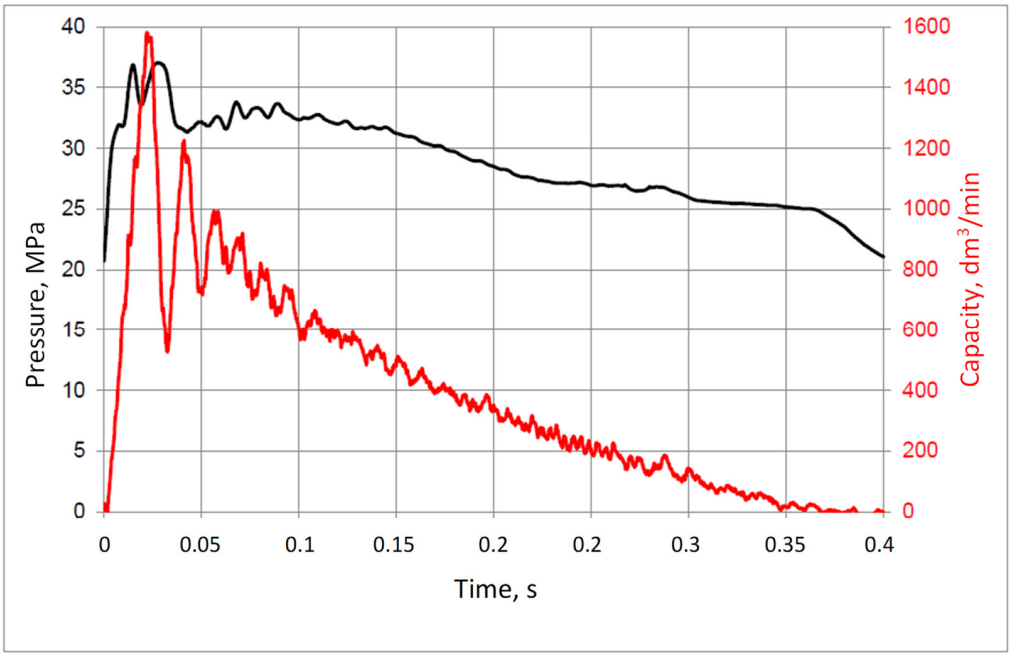

Figure 7. Flow characteristics of the tested valve as a function of time.

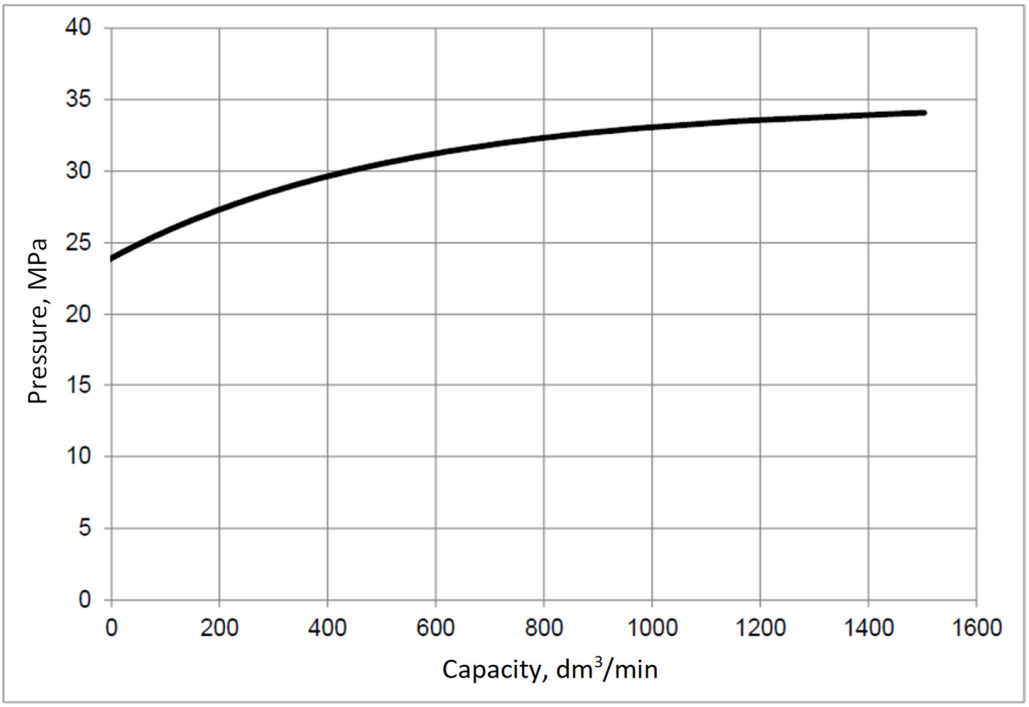

Figure 8. Valve flow characteristics determined using the presented methodology.

The value of the flows for the individual pressures listed is used to assess the load resistance of the powered roof support as a derivative of the rock mass shock. After testing, the valve remained tight and retained its functionality. Characteristics of the valve opening and closing pressure are shown in Figure 9. Based on the above, it can be concluded that even at very high impact energies, there is some delay in the opening of the safety valve. During this time, there is a large increase in the pressure of the liquid in the under-piston space of the prop. This increase in the pressure of the liquid can destroy the powered roof support during the rock mass tremors during its rapid expansion in load on the powered roof support, due to overloading.

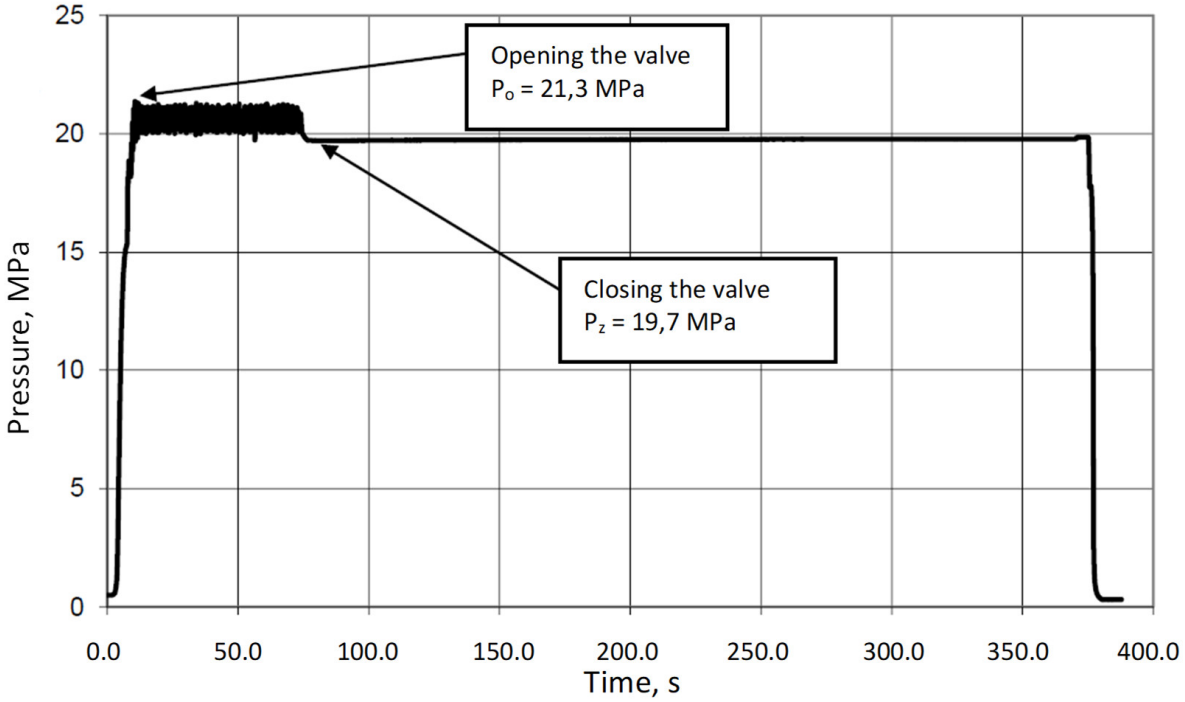

Figure 9. Characterization of valve opening and closing pressures.

4. Discussion

The dynamic testing of the safety valve was carried out with the hydraulic prop using this valve. During the tests, the prop was dynamically loaded. Its protection against damage due to dynamic load relies on limiting the pressure increase in the hydraulic medium inside the prop's cylinder caused by this load by the valve opening quickly at the preset yield load. The test consisted of lowering the ram from a certain height, and hitting the traverse under which the prop is located (Figure 10). In this type of test, the weight of the traverse may have a decisive influence on the test results (Figure 11). The basic instantaneous load of the prop manifests as momentary forces and inertia forces.

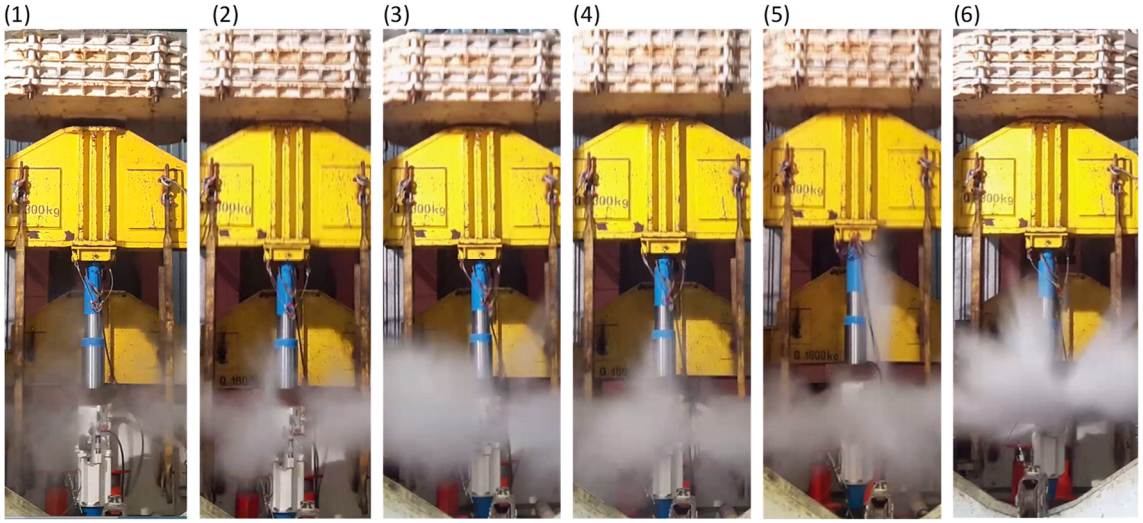

Figure 10. Opening of the safety valve during tests for different heights of impact mass drop, where: (**1**) drop height 20 cm, (**2**) drop height 30 cm, (**3**) drop height 40 cm, (**4**) drop height 50 cm, (**5**) drop height 60 cm, (**6**) drop height 70 cm.

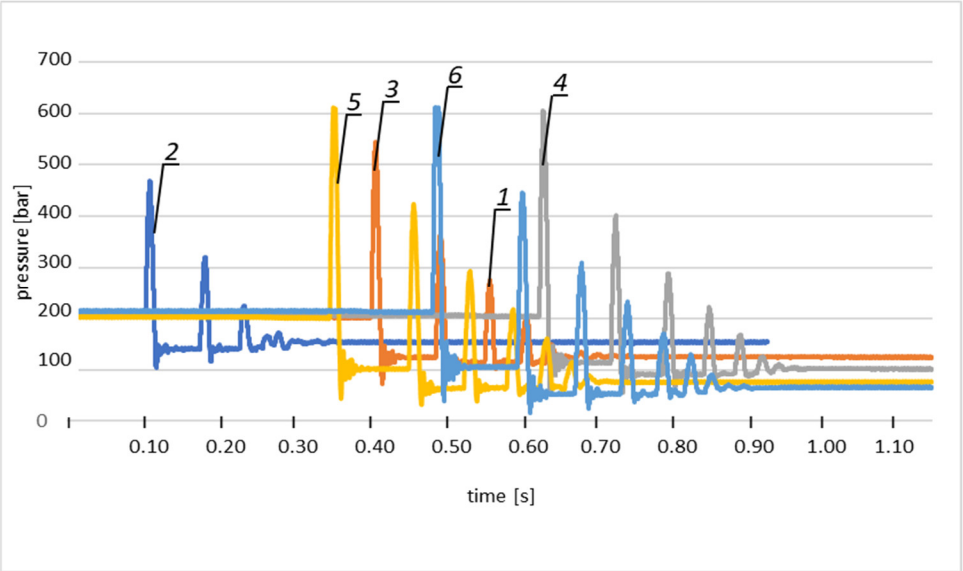

Figure 11. Performance characteristics of the prop, including safety valve loaded with an impact mass freely falling from the following heights, where: 1—drop height 20 cm, 2—drop height 30 cm, 3—drop height 40 cm, 4—drop height 50 cm, 5—drop height 60 cm, 6—drop height 70 cm.

The prop with the safety valve yields under the influence of kinetic energy load. The slip in the prop is more prominent with a larger flow area in the safety valve under test and a smaller flow resistance. The prop's slip and the safety valve's opening time determine the liquid's average pressure in the under-piston space of the stand during the opening of the valve. Accordingly, the flow rate of the liquid through the valve, and its flow resistance, can be determined (Table 1). When the pressure of the liquid exceeds the strength of the cylinder, the prop is destroyed (Figures 2 and 3). The safety valve (Figure 5) connected to the under-piston space of the prop is intended to prevent an excessive increase in fluid pressure in this space.

Table 1. Flow value occurring in the safety valve.

Height of Drop (m)	Energy of Impact Mass E_u (kJ)	Maximum Pressure (bar)	Leg Slide (m)	Flow Value Q(t) (m^3s^{-1})
0.2	58.8	280	0.02	50
0.3	78.4	480	0.03	75
0.4	98.1	550	0.04	100
0.5	117.7	605	0.05	125
0.6	137.3	610	0.06	150
0.7	156.9	620	0.07	175

The kinetic energy transferred by the ram to the tested prop is converted. This is partially for the operation of the prop's slip due to the opening of the tested safety valve, and partly for the elastic energy of the cylinder. The rest of the energy is dissipated due to vibrations in the test stand and resulting shocks. At some time after the impact, the movement of the ram is inhibited, which equates to the loss of the ram's kinetic energy. The prop's slip occurs only during ram impacts, causing the safety valve to open. The energy of the ram on the test site or the roof of the mining excavation transferred to the prop may also cause its slip when the load no longer acts on this prop.

The speed of movement of the prop piston forces the appropriate flow rate of liquid from the prop sub-piston space once the preset pressure has been exceeded. The pressure relief valve must ensure that the flow rate is such that the pressure of the liquid in the under-piston space of the prop at the moment of impact cannot rise too rapidly, so the speed

at which the valve release mechanism opens is very important. The following test results (Figures 6 and 7) show that with a lower flow rate of liquid through the valve than the flow rate of the piston forced by the movement of the prop, a greater increase in the pressure of the liquid in the space under the piston rod of the hydraulic prop will be obtained. On the basis of the above, it can be concluded that even at very high impact energies, there is some delay in the opening of the safety valve, during which there is a sufficiently large increase in the pressure of the liquid in the under-piston space of the prop. This increase in the pressure of the liquid can cause the destruction of the powered roof support during the rock mass tremors during its rapid increase in load on the powered roof support.

5. Conclusions

When performing site tests, one should be aware of the difference between the natural conditions and the conditions of the site tests. In the case of testing a prop with a safety valve, the difference between the dynamic load occurring in the mine excavation and the dynamic load on the test site should be assessed. In underground conditions, the dynamic weight of the roof on the powered roof support is usually greater than its load capacity. In comparison, the weight of the ram (20,000 kg) of the prop is smaller than the nominal load capacity. In addition, the steel ram's elasticity and the prop's foundation differ significantly from the elasticity of the roof rocks and the footwall of the excavation. The speed of the prop load capacity and the powered roof support's load capacity in the excavation at the moment of tremor is also different. Dynamic load in the mining excavation or on the test site causes an increase in the pressure of the liquid in its under-piston space. This increase in liquid pressure is greater the higher the kinetic energy loads on the prop is.

In the longwall complex, the task of the powered roof support is to protect the workers, machines and devices implementing the coal extraction process. It is required of the powered roof support structure, and of the hydraulic prop, that they can carry the dynamic and static loads resulting from the pressure of the rock mass. The impact of the rock mass on the prop (Figure 3) can be assumed as dynamic, which is the result of processes occurring in the rock mass through exploitation.

The bench tests carried out on the prop and the safety valve under dynamic load allowed us to determine the operating range of the safety valve. Bench tests confirm the correct operation of the valve for the adopted test site parameters. The resulting valve opening pressure characteristic was 21.3 MPa. In contrast, the valve closure characteristics were obtained at 19.7 MPa. Both characteristics are shown in Figure 9. As a result, the valve protects the prop against dynamic load. This is important for limiting the effects of rock mass shock. Referring to the impact of rock mass operation on the powered roof support, the adopted parameters of the safety valve operation are insufficient.

Funding: This research received no external funding.

Institutional Review Board Statement: The study was conducted according to the guidelines of the declaration.

Informed Consent Statement: Not applicable.

Data Availability Statement: Not applicable.

Conflicts of Interest: The author declares no conflict of interest.

References

1. Bortnowski, P.; Gładysiewicz, L.; Król, R.; Ozdoba, M. Energy Efficiency Analysis of Copper Ore Ball Mill Drive Systems. *Energies* **2021**, *14*, 1786. [CrossRef]
2. Huang, P.; Spearing, S.; Ju, F.; Jessu, K.V.; Wang, Z.; Ning, P. Control Effects of Five Common Solid Waste Backfilling Materials on In Situ Strata of Gob. *Energies* **2019**, *12*, 154. [CrossRef]
3. Bardzinski, P.; Jurdziak, L.; Kawalec, W.; Król, R. Copper ore quality tracking in a belt conveyor system using simulation tools. *Nat. Resour. Res.* **2020**, *29*, 1031–1040. [CrossRef]
4. Szurgacz, D.; Zhironkin, S.; Cehlár, M.; Vöth, S.; Spearing, S.; Liqiang, M. A Step-by-Step Procedure for Tests and Assessment of the Automatic Operation of a Powered Roof Support. *Energies* **2021**, *14*, 697. [CrossRef]

5. Świątek, J.; Janoszek, T.; Cichy, T.; Stoiński, K. Computational Fluid Dynamics Simulations for Investigation of the Damage Causes in Safety Elements of Powered Roof Supports—A Case Study. *Energies* **2021**, *14*, 1027. [CrossRef]
6. Rajwa, S.; Janoszek, T.; Prusek, S. Influence of canopy ratio of powered roof support on longwall working stability—A case study. *Int. J. Min. Sci. Tech.* **2019**, *29*, 591–598. [CrossRef]
7. Woźniak, D.; Hardygóra, M. Method for laboratory testing rubber penetration of steel cords in conveyor belts. *Min. Sci.* **2020**, *27*, 105–117. [CrossRef]
8. Bajda, M.; Błażej, R.; Hardygóra, M. Optimizing splice geometry in multiply conveyor belts with respect to stress in adhesive bonds. *Min. Sci.* **2018**, *25*, 195–206.
9. Kawalec, W.; Suchorab, N.; Konieczna-Fuławka, M.; Król, R. Specific energy consumption of a belt conveyor system in a continuous surface mine. *Energies* **2020**, *13*, 5214. [CrossRef]
10. Krauze, K.; Mucha, K.; Wydro, T.; Pieczora, E. Functional and Operational Requirements to Be Fulfilled by Conical Picks Regarding Their Wear Rate and Investment Costs. *Energies* **2021**, *14*, 3696. [CrossRef]
11. Kotwica, K.; Stopka, G.; Kalita, M.; Bałaga, D.; Siegmund, M. Impact of Geometry of Toothed Segments of the Innovative KOMTRACK Longwall Shearer Haulage System on Load and Slip during the Travel of a Track Wheel. *Energies* **2021**, *14*, 2720. [CrossRef]
12. Kumar, R.; Singh, A.K.; Mishra, A.K.; Singh, R. Underground mining of thick coal seams. *Int. J. Min. Sci. Tech.* **2015**, *25*, 885–896. [CrossRef]
13. Skrzypkowski, K.; Korzeniowski, W.; Zagórski, K.; Zagórska, A. Modified Rock Bolt Support for Mining Method with Controlled Roof Bending. *Energies* **2020**, *13*, 1868. [CrossRef]
14. Buyalich, G.; Buyalich, K.; Byakov, M. Factors Determining the Size of Sealing Clearance in Hydraulic Legs of Powered Supports. *E3S Web Conf.* **2017**, *21*, 3018. [CrossRef]
15. Buyalich, G.; Byakov, M.; Buyalich, K. Factors Determining Operation of Lip Seal in the Sealed Gap of the Hydraulic Props of Powered Supports. *E3S Web Conf.* **2017**, *41*, 1045. [CrossRef]
16. Wajs, J.; Trybała, P.; Górniak-Zimroz, J.; Krupa-Kurzynowska, J.; Kasza, D. Modern Solution for Fast and Accurate Inventorization of Open-Pit Mines by the Active Remote Sensing Technique—Case Study of Mikoszów Granite Mine (Lower Silesia, SW Poland). *Energies* **2021**, *14*, 6853. [CrossRef]
17. Wodecki, J.; Góralczyk, M.; Krot, P.; Ziętek, B.; Szrek, J.; Worsa-Kozak, M.; Zimroz, R.; Śliwiński, P.; Czajkowski, A. Process Monitoring in Heavy Duty Drilling Rigs—Data Acquisition System and Cycle Identification Algorithms. *Energies* **2020**, *13*, 6748. [CrossRef]
18. Borkowski, P.J. Comminution of Copper Ores with the Use of a High-Pressure Water Jet. *Energies* **2020**, *13*, 6274. [CrossRef]
19. Jixiong, Z.; Spearing, A.J.S.; Xiexing, M.; Shuai, G.; Qiang, S. Green coal mining technique integrating mining-dressing-gas draining-backfilling-mining. *Int. J. Min. Sci. Tech.* **2017**, *27*, 17–27.
20. Juganda, A.; Strebinger, C.; Brune, J.F.; Bogin, G.E. Discrete modeling of a longwall coal mine gob for CFD simulation. *Int. J. Min. Sci. Tech.* **2020**, *30*, 463–469. [CrossRef]
21. Toraño, J.; Diego, I.; Menéndez, M.; Gent, M. A finite element method (FEM)—Fuzzy logic (Soft Computing)—virtual reality model approach in a coalface longwall mining simulation. *Autom. Constr.* **2008**, *17*, 413–424. [CrossRef]
22. Hu, S.; Ma, L.; Guo, J.; Yang, P. Support-surrounding rock relationship and top-coal movement laws in large dip angle fully-mechanized caving face. *Int. J. Min. Sci. Tech.* **2018**, *28*, 533–539.
23. Wang, X.; Xu, J.; Zhu, W.; Li, Y. Roof pre-blasting to prevent support crushing and water inrush accidents. *Int. J. Min. Sci. Tech.* **2012**, *22*, 379–384.
24. Juárez-Ferreras, R.; González-Nicieza, C.; Menéndez-Díaz, A.; Álvarez-Vigil, A.E.; Álvarez-Fernández, M.I. Measurement and analysis of the roof pressure on hydraulic props in longwall. *Int. J. Coal Geol.* **2008**, *75*, 49–62. [CrossRef]
25. Góralczyk, M.; Krot, P.; Zimroz, R.; Ogonowski, S. Increasing Energy Efficiency and Productivity of the Comminution Process in Tumbling Mills by Indirect Measurements of Internal Dynamics—An Overview. *Energies* **2020**, *13*, 6735. [CrossRef]
26. Zimroz, P.; Trybała, P.; Wróblewski, A.; Góralczyk, M.; Szrek, J.; Wójcik, A.; Zimroz, R. Application of UAV in Search and Rescue Actions in Underground Mine—A Specific Sound Detection in Noisy Acoustic Signal. *Energies* **2021**, *14*, 3725. [CrossRef]
27. Ziętek, B.; Banasiewicz, A.; Zimroz, R.; Szrek, J.; Gola, S. A Portable Environmental Data-Monitoring System for Air Hazard Evaluation in Deep Underground Mines. *Energies* **2020**, *13*, 6331. [CrossRef]
28. Wang, J.; Wang, Z. Systematic principles of surrounding rock control in longwall mining within thick coal seams. *Int. J. Min. Sci. Tech.* **2019**, *29*, 591–598. [CrossRef]
29. Ji, Y.; Ren, T.; Wynne, P.; Wan, Z.; Zhaoyang, M.; Wang, Z. A comparative study of dust control practices in Chinese and Australian longwall coal mines. *Int. J. Min. Sci. Tech.* **2016**, *25*, 687–706. [CrossRef]
30. Peng, S.S.; Feng, D.; Cheng, J.; Yang, L. Automation in U.S. longwall coal mining: A state-of-the-art review. *Int. J. Min. Sci. Tech.* **2019**, *29*, 151–159. [CrossRef]
31. Stoiński, K. *Mining Roof Support in Hazardous Conditions of Mining Tremors. Collective Work for Editing Kazimierza Stoińskiego*; The Central Mining Institute: Katowice, Poland, 2018.
32. Adach-Pawelus, K.; Pawelus, D. Influence of Driving Direction on the Stability of a Group of Headings Located in a Field of High Horizontal Stresses in the Polish Underground Copper Mines. *Energies* **2021**, *14*, 5955. [CrossRef]
33. Dlouhá, D.; Dubovský, V. The improvement of the lake Most evaporation estimates. *Inżynieria Miner.* **2019**, *21*, 159–164.

34. Klishin, V.I.; Klishin, S.V. Coal Extraction from Thick Flat and Steep Beds. *J. Min. Sci.* **2010**, *46*, 149–159. [CrossRef]
35. Ralston, J.C.; Reid, D.C.; Dunn, M.T.; Hainsworth, D.W. Longwall automation: Delivering enabling technology to achieve safer and more productive underground mining. *Int. J. Min. Sci. Tech.* **2015**, *25*, 865–876. [CrossRef]
36. Ralston, J.C.; Hargrave, C.O.; Dunn, M.T. Longwall automation: Trends, challenges and opportunities. *Int. J. Min. Sci. Tech.* **2017**, *27*, 733–739. [CrossRef]
37. Janus, J.; Krawczyk, J. Measurement and Simulation of Flow in a Section of a Mine Gallery. *Energies* **2021**, *14*, 4894. [CrossRef]
38. Prostański, D. Empirical Models of Zones Protecting Against Coal Dust Explosion. *Arch. Min. Sci.* **2017**, *62*, 611–619. [CrossRef]
39. Grzesiek, A.; Zimroz, R.; Śliwiński, P.; Gomolla, N.; Wyłomańska, A. A Method for Structure Breaking Point Detection in Engine Oil Pressure Data. *Energies* **2021**, *14*, 5496. [CrossRef]
40. Patyk, M.; Bodziony, P.; Krysa, Z. A Multiple Criteria Decision Making Method to Weight the Sustainability Criteria of Equipment Selection for Surface Mining. *Energies* **2021**, *14*, 3066. [CrossRef]
41. Król, R.; Kisielewski, W. Research of loading carrying idlers used in belt conveyor-practical applications. *Diagnostyka* **2014**, *15*, 67–74.
42. Kawalec, W.; Błażej, R.; Konieczna, M.; Król, R. Laboratory Tests on e-pellets effectiveness for ore tracking. *Min. Sci.* **2018**, *25*, 7–18.
43. Doroszuk, B.; Król, R. Analysis of conveyor belt wear caused by material acceleration in transfer station. *Min. Sci.* **2019**, *26*, 189–201. [CrossRef]
44. Szurgacz, D.; Zhironkin, S.; Vöth, S.; Pokorný, J.; Spearing, A.J.S.; Cehlár, M.; Stempniak, M.; Sobik, L. Thermal Imaging Study to Determine the Operational Condition of a Conveyor Belt Drive System Structure. *Energies* **2021**, *14*, 3258. [CrossRef]
45. Bajda, M.; Hardygóra, M. Analysis of Reasons for Reduced Strength of Multiply Conveyor Belt Splices. *Energies* **2021**, *14*, 1512. [CrossRef]
46. Gładysiewicz, L.; Król, R.; Kisielewski, W.; Kaszuba, D. Experimental determination of belt conveyors artificial friction coefficient. *Acta Montan. Slovaca* **2017**, *22*, 206–214.
47. Buyalich, G.; Byakov, M.; Buyalich, K.; Shtenin, E. Development of Powered Support Hydraulic Legs with Improved Performance. *E3S Web Conf.* **2019**, *105*, 3025. [CrossRef]
48. Stoiński, K.; Mika, M. Dynamics of Hydraulic Leg of Powered Longwall Support. *J. Min. Sci.* **2003**, *39*, 72–77. [CrossRef]
49. Frith, R.C. A holistic examination of the load rating design of longwall shields after more than half a century of mechanised longwall mining. *Int. J. Min. Sci. Tech.* **2015**, *26*, 199–208. [CrossRef]
50. Qiao, S.; Zhang, Z.; Zhu, Z.; Zhang, K. Influence of cutting angle on mechanical properties of rock cutting by conical pick based on finite element analysis. *J. Min. Sci.* **2021**, *28*, 161–173.
51. Pokorny, J.; Dlouhá, D.; Kucera, P. Study of the necessity of use virtual origin in assessment of selected fire plume characteristics. *MM Sci. J.* **2016**, *5*, 1424–1428. [CrossRef]
52. Uth, F.; Polnik, B.; Kurpiel, W.; Baltes, R.; Kriegsch, P.; Clause, E. An innovate person detection system based on thermal imaging cameras dedicate for underground belt conveyors. *Min. Sci.* **2019**, *26*, 263–276.
53. Dlouhá, D.; Dubovský, V.; Pospíšil, L. Optimal calibration of evaporation models against Penman-Monteith equatíon. *Water* **2021**, *13*, 1484. [CrossRef]
54. Dubovský, V.; Dlouhá, D.; Pospíšil, L. The calibration of evaporation models against the Penman-Monteith equation on lake Most. *Sustainability* **2021**, *13*, 313. [CrossRef]
55. Szurgacz, D. Dynamic Analysis for the Hydraulic Leg Power of a Powered Roof Support. *Energies* **2021**, *14*, 5715. [CrossRef]
56. Dlouhá, D.; Hamříková, R. Our experience with the involvement of students in the creation of study materials. In Proceedings of the 17th Conference on Applied Mathematics, Bratislava, Slovakia, 6–8 February 2018; Volume 1, pp. 301–308.
57. Pokorny, J.; Mozer, V.; Malerova, L.; Dlouhá, D.; Wilkinson, P. A simplified method for establishing safe available evacuation time based on a descending smoke layer. *Commun.-Sci. Lett. Univ. Zilina* **2018**, *20*, 28–34. [CrossRef]
58. Zhao, X.; Li, F.; Li, Y.; Fan, Y. Fatigue Behavior of a Box-Type Welded Structure of Hydraulic Support Used in Coal Mine. *Materials* **2015**, *8*, 6609–6622. [CrossRef]
59. Dlouhá, D.; Hamříková, R. Interactive distance materials of mathematics for VŠB-TU Ostrava. In *Overcoming the Challenges and the Barriers in Open Education*; DisCo; Centre for Higher Education Studies: Prague, Czech Republic, 2018; pp. 67–72.
60. Dlouhá, D.; Pokorný, J.; Dlouhá, K. Necessity of knowledge about math in safety engineering. In *E- Learning: Unlocking the Gate to Education around the Globe*; DisCo; Centre for Higher Education Studies: Prague, Czech Republic, 2019; pp. 380–386.
61. Bazaluk, O.; Slabyi, O.; Vekeryk, V.; Velychkovych, A.; Ropyak, L.; Lozynskyi, V. A Technology of Hydrocarbon Fluid Production Intensification by Productive Stratum Drainage Zone Reaming. *Energies* **2021**, *14*, 3514. [CrossRef]
62. Bazaluk, O.; Velychkovych, A.; Ropyak, L.; Pashechko, M.; Pryhorovska, T.; Lozynskyi, V. Influence of Heavy Weight Drill Pipe Material and Drill Bit Manufacturing Errors on Stress State of Steel Blades. *Energies* **2021**, *14*, 4198. [CrossRef]
63. Zhou, R.; Meng, L.; Yuan, X.; Qiao, Z. Research and Experimental Analysis of Hydraulic Cylinder Position Control Mechanism Based on Pressure Detection. *Machines* **2022**, *10*, 1. [CrossRef]
64. Ren, H.; Zhang, D.; Gong, S.; Zhou, K.; Xi, C.; He, M.; Li, T. Dynamic impact experiment and response characteristics analysis for 1:2 reduced-scale model of hydraulic support. *Int. J. Min. Sci. Technol.* **2021**, *31*, 347–356. [CrossRef]
65. Dlouhá, D.; Kozlová, K. Knowledge assessment of student's high school mathematics. In Proceedings of the 17th Conference on Applied Mathematics, Bratislava, Slovakia, 5–7 February 2019; Volume 1, pp. 243–252.

66. Hamříková, R.; Dlouhá, D. Video tutorials for students of the master's program. In *Open Education as a Way to a Knowledge Society*; DisCo; Centre for Higher Education Studies: Prague, Czech Republic, 2017; pp. 446–451.
67. Ji, Y.; Zhang, Y.; Huang, Z.; Shao, Z.; Gao, Y. Theoretical analysis of support stability in large dip angle coal seam mined with fully-mechanized top coal caving. *Min. Sci.* **2020**, *27*, 73–87. [CrossRef]
68. Baiul, K.; Khudyakov, A.; Vashchenko, S.; Krot, P.V.; Solodka, N. The experimental study of compaction parameters and elastic after-effect of fine fraction raw materials. *Min. Sci.* **2020**, *27*, 7–18. [CrossRef]
69. Szurgacz, D.; Brodny, J. An innovative system to test components of mining machinery control hydraulics. In Proceedings of the 17th International Multidisciplinary Scientific Geoconference SGEM, Albena, Bulgaria, 29 June–5 July 2017. [CrossRef]